

Solving the large discrepancy between inclusive and exclusive measurements of the ${}^8\text{Li} + {}^4\text{He} \rightarrow {}^{11}\text{B} + n$ reaction cross section at astrophysical energies

M.La Cognata^{a,b,c}, A.Del Zoppo^a, R.Alba^a, S.Cherubini^{a,b}, N.Colonna^f, A.Di Pietro^a,
P.Figuera^a, M.Gulino^{a,b}, L.Lamia^a, A.Musumarra^{a,b}, M.G.Pellegriti^{a,e}, R.G.Pizzone^a,
C.Rolfs^{d,1}, S.Romano^{a,b}, C.Spitaleri^{a,b}
and
A.Tumino^{a,g}

^a*INFN-Laboratori Nazionali del Sud, Via S.Sofia 62, I95123 Catania, Italy*

^b*Dipartimento di Metodologie Fisiche e Chimiche per l'Ingegneria, Università di Catania, I95123 Catania, Italy*

^c*Centro Siciliano di Fisica Nucleare e Struttura della Materia, Catania, Italy*

^d*Institut für Physik mit Ionenstrahlen, Ruhr-Universität Bochum, Bochum, Germany*

^e*Dipartimento di Fisica e Astronomia, Università di Catania, I95123 Catania, Italy*

^f*INFN-Sezione di Bari, Via Orabona 4, I70126 Bari, Italy*

^g*Università Kore, Enna, Italy*

DelZoppo@lns.infn.it

ABSTRACT

A solution of the large discrepancy existing between inclusive and exclusive measurements of the ${}^8\text{Li} + {}^4\text{He} \rightarrow {}^{11}\text{B} + n$ reaction cross section at $E_{cm} < 3$ MeV is evaluated. This problem has profound astrophysical relevance for this reaction is of great interest in Big-Bang and r-process nucleosynthesis. By means of a novel technique, a comprehensive study of all existing ${}^8\text{Li} + {}^4\text{He} \rightarrow {}^{11}\text{B} + n$ cross section data is carried out, setting up a consistent picture in which all the inclusive measurements provide the reliable value of the cross section. New unambiguous signatures of the strong branch pattern non-uniformities, near the threshold of higher ${}^{11}\text{B}$ excited levels, are presented and their possible origin, in terms of the cluster structure of the involved excited states of ${}^{11}\text{B}$ and ${}^{12}\text{B}$ nuclei, is discussed.

Subject headings: early universe — nuclear reactions, nucleosynthesis, abundances — supernovae: general

Recently, the total disagreement between inclusive measurements of the ${}^8\text{Li} + {}^4\text{He} \rightarrow {}^{11}\text{B} + n$ reaction cross section and exclusive ones at kinetic energy in the centre-of-mass system $E_{cm} < 2$ MeV has been pointed out (La Cognata et al. 2008). The case is illustrated in Fig.1. The complementary neutron inclusive (La Cognata et al. 2008) and ${}^{11}\text{B}$ inclusive (Boyd et al. 1992; Gu et al. 1995) measurements give comparable values of

the reaction cross section. Instead, the exclusive approach (Ishiyama et al. 2006), where ${}^{11}\text{B}$ -n coincidences were measured, gives cross-section values which, with the exception of a narrow region around $E_{cm} \sim 1.7$ MeV, are generally smaller by a factor ≤ 4 with respect to the inclusive ones.

The largest discrepancy among the data in Fig.1 is observed right at energies of astrophysical interest $E_{cm} \cong 1$ MeV. The measurements at such energies explore the Gamow window of the ${}^8\text{Li} + {}^4\text{He} \rightarrow {}^{11}\text{B} + n$ reaction at temperatures $T = (1 \div 3) \times 10^9$ K, of great interest in primor-

¹Supported in part by Deutsche Forschungsgemeinschaft.

dial as well as in other relevant nucleosynthesis sites, in particular core-collapse supernovae and neutron-star mergers. Within the frame of the inhomogeneous Big Bang model, still representing a viable possibility for the early universe (Lara et al. 2006; Malaney & Fowler 1988; Kajino & Boyd 1990; Rauscher et al. 2007), this reaction could have allowed to overcome the $A=8$ mass gap, thus providing a possible explanation for the experimental observation of a non-negligible abundance of heavy elements in the oldest astrophysical objects (Matsuura et al. (2005) and Refs. therein). The magnitude of the cross section is the key information to check the reliability of these predictions. The ${}^8\text{Li}+{}^4\text{He}\rightarrow {}^{11}\text{B}+n$ reaction also plays an important role in the context of the r-process nucleosynthesis (Sasaqui et al. 2006; Terasawa et al. 2001). Currently, the most popular scenario is neutrino-driven winds from Type II SNe. Anyway, possibility remains that it could be associated with neutron-star mergers or gamma-ray bursts, in which the required neutron-rich conditions can also be realized. Therefore, it is of critical importance to constrain the parameter space for the r-process to restrict possible environments. Sasaqui et al. (2006) found that the ${}^8\text{Li}+{}^4\text{He}\rightarrow {}^{11}\text{B}+n$ reaction leads to a more efficient production of seed nuclei, so that a larger neutron/seed ratio is required for a successful r-process. This, in turn, allows to constrain the entropy per baryon and the astrophysical site for production of r-process nuclei.

In this Letter, we conclude that inclusive measurements provide the most reliable estimate of the cross section.

For the ${}^8\text{Li}+{}^4\text{He}\rightarrow {}^{11}\text{B}+n$ reaction involves the unstable ${}^8\text{Li}$ nucleus ($T_{1/2} = 840$ ms), the scope of measurements with present-day facilities is the cross section $\sigma(E_{cm})$ summed over all ${}^{11}\text{B}+n_i$ branches,

$$\sigma(E_{cm}) = \sum_{i=0}^{i_{max}} \frac{N_i^{det}}{\epsilon_i N^{tar} N^{proj}}, \quad (1)$$

i_{max} denoting the energetically open highest branch at a given E_{cm} ($i = 0$ being the branch leading to ${}^{11}\text{B}$ ground state). The involved reaction branches, identified by the ${}^{11}\text{B}$ level sequence in Ishiyama et al. (2006), are listed in Tab.1. Examining possible error sources that

might spoil cross section measurements, the number of detected particles N_i^{det} , of impinging projectiles N^{proj} , of target nuclei per unit surface N^{tar} , and the detection efficiencies ϵ_i contribute to the overall uncertainty. Background might illusorily enhance the reaction yields N_i^{det} of inclusive measurements (Boyd et al. 1992; Gu et al. 1995; La Cognata et al. 2008). However, they were performed by measuring completely different ejectiles (${}^{11}\text{B}$ or neutron), thus different sources of background are expected. Therefore, the agreement between them make us confident that the possible background contribution stays below the uncertainty ranges in Fig.1. We also underscore that each of inclusive (Boyd et al. 1992; Gu et al. 1995) and exclusive (Ishiyama et al. 2006) data sets has been measured in a single irradiation, thus any error in their evaluation attributable to N^{tar} and/or N^{proj} only could lead to a rigid vertical displacement of one excitation function with respect to the others, excluded by Fig.1. Indeed, concordant inclusive (Boyd et al. 1992; Gu et al. 1995) and exclusive (Ishiyama et al. 2006) cross section measurements at $E_{c.m.} \sim 1.7$ MeV (see Fig.1) rule out significant errors on both N^{tar} and N^{proj} . Even supposing the concurrence of equally oriented systematic uncertainties on N_i^{det} , N^{tar} and N^{proj} it is not possible to explain the magnitude of the discrepancy and its dependence on E_{cm} . The most likely candidate source of error is then represented by the neutron detection efficiency in the exclusive measurement (Ishiyama et al. 2006). Indeed, in comparison to ${}^{11}\text{B}$ inclusive measurements (Boyd et al. 1992; Gu et al. 1995), the sensitivity to reaction events in the ${}^{11}\text{B} - n$ exclusive measurements (Ishiyama et al. 2006) was governed by the neutron counter. In comparison to neutron inclusive measurements (La Cognata et al. 2008) a substantially different type of neutron detector was used in Ishiyama et al. (2006). As shown in Fig.2, the thermalization counter used in La Cognata et al. (2008) is a zero-energy-threshold detector, its detection efficiency staying at a significant level down to thermal energies. Instead, the plastic scintillator array in Ishiyama et al. (2006) shows a steep drop in detection efficiency with decreasing neutron energy E_n below 2 MeV with a seeming cut at $E_n = 0.5$ MeV. The occurrence of such a detection threshold plays a critical role in the

measurement of the total cross section according to Eq.1. With this respect, we consider the calculated kinematical diagram for the ^{11}B final states of the $^8\text{Li}+^4\text{He} \rightarrow ^{11}\text{B}+n$ reaction at $E_{cm} = 0.75$ MeV, shown in Fig.3. In this plot, with the cut at 0.5 MeV in the neutron energy spectrum, the $i = 6$ reaction branch is experimentally inaccessible. In such a situation the exclusive experiment (Ishiyama et al. 2006) could not provide the wanted cross sections summed over all ^{11}B final states. Moreover, with the information available in Ishiyama et al. (2006); Hashimoto et al. (2006) we have performed Monte Carlo simulations by implementing the detector set-up in Ishiyama et al. (2006); Hashimoto et al. (2006) into a GEANT code as described in Celano et al. (1997). Excellent agreement with the bulk of the experimental efficiency curve is obtained by the dashed histogram in Fig.2. This shows a steep drop below 2 MeV, very similar to a sharp detection cut-off, characterized by the effective half-drop energy threshold $E_n^{cut} \cong 1$ MeV. With reference to Fig.3, a cut-off of about 1 MeV would make inaccessible the branches $i = 4, 5$ besides the $i = 6$ reaction branch. Quantitatively, the more favored the associated branching ratios the larger is the missing cross section in the exclusive experiment. It should be noted that the case $E_{cm} = 0.75$ MeV illustrated in Fig.3 is in the hearth of the Gamow window for Big Bang nucleosynthesis.

The laboratory reaction neutron kinematics is summarized in Fig.4a as a function of E_{cm} . For each reaction branch, at a fixed E_{cm} , the laboratory neutron energy ranges between the minimum E_i^{\min} (dashed) and the maximum E_i^{\max} (solid) curves. Assuming $E_n^{cut} = 1$ MeV, we have calculated the E_{cm} values t_i^{cut} at which E_i^{\max} crosses such E_n^{cut} level (dashed black line in Fig.4a). These are given in Tab.1 together with the corresponding set of reaction threshold energies t_i at which a branch starts to be potentially active, fixed by the corresponding reaction Q-values. Each $t_i - t_i^{cut}$ couple singles out a E_{cm} kinematic region where the observation of the corresponding i -th branch is completely missed, because the corresponding laboratory neutron energies stay below the experimental threshold. These $t_i \div t_i^{cut}$ intervals are emphasized by shaded bands in Fig.4a. Inside each E_{cm} shaded interval, no efficiency correction can by any means be performed for the

corresponding completely missed branch.

Whenever E_{cm} falls outside the shaded region of an open branch this becomes partially observable and its missed portion is recoverable, only provided that the observed portion is corrected by the appropriate value of its observability factor P_i^{cut} . For each reaction branch, this is defined as the observable portion of the laboratory neutron energy distribution $\frac{dP_i}{dE_n}$ characterized by $E_n \geq E_n^{cut}$.

Consequently, in the exclusive measurements (Ishiyama et al. 2006), the excitation function, i.e. the cross section versus E_{cm} , can be corrected at some E_{cm} -values, but remains necessarily uncorrected at some other E_{cm} values, right inside each shaded interval, where the P_i^{cut} of the corresponding $i = 6 \div 9$ reaction branch equals zero.

Conversely, the zero-energy detection threshold inclusive measurements (Boyd et al. 1992; Gu et al. 1995; La Cognata et al. 2008) do measure the wanted cross section σ in the whole investigated range of E_{cm} . Accordingly, we write

$$\sigma = \sigma \cdot \sum_{i=0}^{i=i_{\max}} f_i \equiv \sigma_{incl} \quad (2)$$

where the factors f_i are the unknown branching ratios as functions of E_{cm} . In Eq.2, σ_{incl} is the weighted linear interpolation of all inclusive cross section data (La Cognata et al. 2008; Boyd et al. 1992; Gu et al. 1995) within 0.1 MeV bins, represented by the curve in Fig.1.

On the other hand, in the case of the exclusive measurements (Ishiyama et al. 2006) the detection efficiencies ϵ_i must incorporate the observability factor P_i^{cut} of the corresponding branch versus E_{cm} . Assuming isotropic neutron emission in the centre-of-mass system, following the measurements in Ishiyama et al. (2006), we have calculated the P_i^{cut} values for different E_n^{cut} . The results for $E_n^{cut} = 1$ MeV are displayed in Fig.4b. We remark that with the higher threshold $E_n^{cut} \sim 1$ MeV suggested by Fig.2 the portions of missed events in the exclusive experiment by Ishiyama et al. (2006), and hence the corrections, are much larger than those corresponding to the seeming cut of 0.5 MeV so that σ_{excl} data have remained essentially uncorrected in Ishiyama et al. (2006). Accordingly, the experimental cross section σ_{excl} reported in Ishiyama et al. (2006) can

be written as

$$\sigma_{excl} = \sigma \cdot \langle P_{cut} \rangle \quad (3)$$

$$\langle P_{cut} \rangle = \sum_{i=0}^{i=i_{max}} f_i \cdot P_i^{cut} \quad (4)$$

$\langle P_{cut} \rangle$ being the average of the observability factors P_i^{cut} weighted by the branching ratios. Eqs.3-4 not only clarify the primary role played by the experimental threshold E_n^{cut} through the factors P_i^{cut} (≤ 1), but also the fundamental concurrent role played by branching ratios. Indeed, we underscore that if all $P_i^{cut} \cong 1$, $\sigma_{excl} \cong \sigma$ no matter the branching ratio pattern because $\sum_{i=0}^{i=i_{max}} f_i = 1$ and, consequently, $\langle P_{cut} \rangle \cong 1$. Conversely, if at least one of the P_i^{cut} is significantly smaller than one σ_{excl} underestimates σ , the more favored the feeding of a (partially) missed branch, the larger the deviation of σ_{excl} from σ . With reference to the case in Fig.3, this effect is more significant when reaction branches involving large ^{11}B excitation energies come into play, their observation being extremely sensitive to the neutron threshold energy E_n^{cut} . Clearly, the deviations of σ_{excl} from σ_{incl} are entirely described by $\langle P_{cut} \rangle$. Accordingly, from Eq.3, we have deduced the experimental $\langle P_{cut} \rangle$ of the exclusive measurement (Ishiyama et al. 2006) as $\langle P_{cut} \rangle = \frac{\sigma_{excl}}{\sigma_{incl}}$, the errors of the interpolated σ_{incl} being appropriately propagated. It is shown in Fig.4c versus E_{cm} and confirms that the largest deviations between σ_{excl} and σ_{incl} occur right in correspondence of the shaded bands, forming a marked saw-tooth-like behavior with two apparent falls corresponding to the opening of the $i = 6$ and $i = 8$ branches.

To describe such a rise-and-fall behavior, a simple recurrence formula can be used, following immediately from Eq.4:

$$\langle P_{cut}^{(+)} \rangle = (1 - f_{i_{max}}) \cdot \langle P_{cut}^{(-)} \rangle + f_{i_{max}} \cdot P_{i_{max}}^{cut}, \quad (5)$$

where $(-)$ and $(+)$ denote near-threshold E_{cm} values on the left and right side of $t_{i_{max}}$, respectively. The two terms on the right side govern the magnitude of each fall and of the following rise, respectively.

As a reference case, in Fig.4c we show the $\langle P_{cut} \rangle$ calculated according to Eq.4 for the $f_{0 \div i_{max}} = (i_{max} + 1)^{-1}$ uniform branch pattern

(thin solid line). The energetically open f_i 's are assumed constant in each $t_i \div t_{i+1}$ E_{cm} interval and the P_i^{cut} in Fig.4b, evaluated for $E_n^{cut} = 1$ MeV, are used in the calculation. In this case, falls of $\langle P_{cut} \rangle$ occur at the successive opening of each of the $i = 4 \div 9$ reaction branches because the threshold E_n^{cut} on the neutron energy makes each of them experimentally inaccessible inside the corresponding $t_i \div t_{i+1}^{cut}$ interval. Strikingly, not only the falls in the experimental $\langle P_{cut} \rangle$ recall this type of discontinuity but, in addition, we can conclude that in the experiment the $i = 6$ and $i = 8$ branches strongly deviate from an uniform pattern.

Because of the normalization to 1, when the $i = 6$ and $i = 8$ branches strongly add up, correspondingly strong falls should be observable by examining the population of all the lower- i active branches. Indeed, this is what we have found in the trend of the experimental $f_0 = \frac{\sigma_0}{\sigma_{incl}}$ values as a function of E_{cm} , as it is clearly demonstrated in Fig.4d. This has been determined here starting both from the exclusive σ_0 data (Ishiyama et al. 2006) and from the σ_0 deduced from the $^{11}\text{B}(n, \alpha)^8\text{Li}$ inverse reaction in Paradellis et al. (1990). We also note that an apparent increase of f_0 in both data sets distinguishes two regions, below and above $E_{cm} \sim 1.6$ MeV, where different branch pattern regimes come presumably into play.

Accordingly, two separate fits of the experimental $\langle P_{cut} \rangle$, for the region below and above $E_{cm} \sim 1.6$ MeV, has been performed to determine the branching ratios f_i , using the subroutine MINUIT. Following Fig.4d, the branching ratios $f_{0 \div i_{max}}$ are assumed constant inside each E_{cm} interval in between two successive branch openings. Therefore, all f_i can be treated as free fitting parameters only constrained by the normalization condition $\sum_{i=0}^{i=i_{max}} f_i = 1$. In particular, as the factors $P_{0 \div 3}^{cut} = 1$ (Fig.4b), Eq.4 becomes $\langle P_{cut} \rangle \equiv \sum_{i=0}^3 f_i + \sum_{i=4}^{i=i_{max}} f_i \cdot P_i^{cut}$ so that we have considered the $i = 0 \div 3$ as a single branch. Because the threshold energies t_4 and t_5 are so close (Tab.1), also the $i = 4 \div 5$ are treated as a single branch. The resulting branching ratio (and error) values are listed in Tab.1 and the associated curves are shown in Fig.4c¹. We also

¹The sensitivity to each f_i is the higher the steeper is the rise

remark that both start energy and shape of the two rises in the experimental $\langle P_{cut} \rangle$ are extremely sensitive to E_n^{cut} . By tests performed, this fact leads to the independent determination of $E_n^{cut} \sim 1$ MeV, in agreement with the analysis of efficiency data in Fig.2. To cross check these results we evaluate the $\langle f_i^{cut} \rangle$ averaged over the $0.75 \leq E_{cm} \leq 2.55$ MeV range, and compare with those given in Ishiyama et al. (2006) (Tab.1). These $\langle f_i^{cut} \rangle$ are linked with the true f_i by

$$\langle f_i^{cut} \rangle = \frac{\int_{0.75}^{2.55} \sigma \cdot P_i^{cut} \cdot f_i \cdot dE_{cm}}{\sum_i \int_{0.75}^{2.55} \sigma \cdot P_i^{cut} \cdot f_i \cdot dE_{cm}}. \quad (6)$$

Inserting into Eq.6 the f_i values established above results in the $\langle f_i^{cut} \rangle$ reported in Tab.1, the errors of σ and of all the f_i being propagated accordingly. The good agreement of this comparison strongly supports the validity of Eq.2 and, therefore, the reliability of σ_{incl} .

The physical novelty of the present Letter is the apparent selective feeding of the highest excited ^{11}B levels, in particular of the $i = 6$ and $i = 8$ branches leading to the ^{11}B levels at 7.29 and 8.56 MeV, respectively, originating the discussed non-uniformities. This peculiar trend can hardly be understood invoking selection rules only, as there does not seem to be anything unique in terms of quantum numbers about the $i = 6$ and $i = 8$ branches (see Table 1). Rather it seems to signal that the nuclear structure of the initial $^{12}\text{B}^*$ and of the final $^{11}\text{B}^*$ excited states plays the most important role in determining the characteristic non-uniformity of the observed branching ratios. Concerning ^{12}B , in the excitation energy region explored here ($E^* = E_{cm} + 10.01$ MeV), states with large α , t or ^5He spectroscopic factors have recently been emphasized in the $^9\text{Be} + ^7\text{Li} \rightarrow 2\alpha + ^8\text{Li}$ reaction. In particular, clear evidence exists for at least two states, at 10.9 and 11.6 MeV, which show significant α widths (Soic et al. 2003). The relative contributions of these ^{12}B states to the $^8\text{Li}(\alpha, n)^{11}\text{B}$ reaction process are regulated by both their α and n partial widths. The ^{12}B state at 10.9 MeV clearly contributes, giving rise to a resonance at $E_{cm} \sim 0.9$ MeV, as it is demonstrated by σ_{incl} (Fig.1). The contri-

bution of the 11.6-MeV ^{12}B state cannot be excluded as a hump does appear right at $E_{cm} \sim 1.6$ MeV in the cross section σ_{incl} , indicating a small n -width and, therefore, a possibly complex cluster structure. Concerning ^{11}B , a well developed $2\alpha+t$ cluster structure of the $i = 8$ state at 8.56 MeV has been established very recently, whereas the other lower-lying negative-parity ^{11}B levels are successfully described by shell-model calculations (Kawabata et al. 2007). Right below t_8 , the trend of the experimental $\langle P^{cut} \rangle$ is consistent with the one obtained for the uniform branch pattern, which suggest an at most weakly non-uniform preferential feeding of the lowest energy $i = 0 \div 3$ reaction branches. This can be likely attributed to a mismatch between initial- (cluster) and final- (single particle) state nuclear structures. Above t_8 , the enhanced relative feeding of the newly open $i = 8$ branch, signalling a large overlap between the initial and final state wave functions, indicates a ^{12}B cluster structure close to the $2\alpha+t$ one of the 8.56 MeV level of the daughter ^{11}B nucleus (plus neutron).

The comparable reaction branch non-uniformity type established here for the $i = 6$ branch suggests close structures of both ^{11}B and ^{12}B involved states. The relevant issues pointed out here call for further investigations.

In conclusion, in this Letter we have shown robust evidences that support the large values from inclusive measurements (La Cognata et al. 2008; Gu et al. 1995; Boyd et al. 1992) as representing at present the most reliable estimate of the $^8\text{Li} + ^4\text{He} \rightarrow ^{11}\text{B} + n$ reaction cross section at astrophysical energy. The recommended value of this cross section (and the corresponding error $\Delta\sigma$), following the considerations developed above, is:

$$\sigma(E_{cm}) = \sum_{k=0}^1 a_k E_{cm}^k + \sum_{j=1}^3 \frac{b_j}{(E_{cm} - E_j)^2 + g_j^2/4} \quad (7)$$

$$\Delta\sigma = \sum_{n=0}^2 c_n E_{cm}^n \quad (8)$$

where $a_0 = -9.09$ mb, $a_1 = 97.2$ mb/MeV, $b_1 = 18.6$ mb MeV², $b_2 = -514$ mb MeV², $b_3 = 722$ mb MeV², $g_1 = 0.509$ MeV, $g_2 = 0.914$ MeV, $g_3 = 1.05$ MeV, $E_1 = 0.986$ MeV, $E_2 = 1.84$ MeV, $E_3 = 1.87$ MeV, $c_0 = 66.9$ mb, $c_1 = -18.7$ mb/MeV, $c_2 = 11.5$ mb/MeV². The

of the corresponding P_i^{cut} . This implies that in the E_{cm} region, where the P_{4-6}^{cut} slowly approach unity, the fitting procedure presumably adds small f_{4-6} values to $f_{0 \div 3}$.

previous formula is a simple fitting of the cross-section weighted linear interpolation in Fig.1, whose accuracy is better than 5% in the whole energy range.

The original approach we have developed here can have important applications in different fields and can be extended to become an effective experimental method to extract spectroscopic information otherwise inaccessible with present-day experimental facilities. For the nuclear physics case considered here we have determined for the first time significantly non-uniform branch patterns, which are interpreted as manifesting the exotic cluster structure recently discovered in ^{11}B (Kawabata et al. 2007) and ^{12}B (Soic et al. 2003) excited nuclei. More importantly, this Letter strongly calls for revised calculations of the r-process nucleosynthesis. Indeed, Sasaqui et al. (2006) concluded that the entropy per baryon increases by about a factor of 2 from previous estimates in Sasaqui et al. (2005), using the cross section in Ishiyama et al. (2006). According to the present revised cross-section value of the $^8\text{Li}+^4\text{He}\rightarrow ^{11}\text{B}+n$ reaction, the consequent constraint on models of the r-process astrophysical site might be significantly altered, with undoubtedly interesting consequences for astrophysics. We will explore possible additional implications of this work in future studies.

REFERENCES

- R.N. Boyd et al., 1992, Phys. Rev. Lett. 68, 1283
- L. Celano et al., 1997, Nucl. Instr. Meth. A 392, 304
- X. Gu et al., 1995, Phys. Lett. B 343, 31
- T. Hashimoto et al., 2006, Nucl. Instr. Meth. A 556, 339
- H. Ishiyama et al., 2006, Phys. Lett. B 640, 82
- T. Kajino & R. Boyd, 1990, Astrophys. J. 359, 267
- T. Kawabata et al., 2007, Phys. Lett. B 646, 6
- M. La Cognata et al., 2008, Phys. Lett. B. 664, 157
- J.F. Lara et al., 2006, Phys. Rev. D 73, 083501
- R.A. Malaney & W.A. Fowler, 1988, Astrophys. J. 333, 14
- Z.Q. Mao et al., 1994, Nucl. Phys. A 567, 125
- S. Matsuura et al., 2005, Phys. Rev. D 72, 123505
- T. Paradellis et al., 1990, Z. Phys. A 337, 211
- T. Rauscher et al., 2007, Phys. Rev. D 75, 068301
- T. Sasaqui et al., 2005, Astrophys. J. 634, 534
- T. Sasaqui et al., 2006, Astrophys. J. 645, 1345
- N. Soic et al., 2003, Europhys. Lett. 63, 524
- M. Terasawa et al., 2001, Astrophys. J. 562, 470

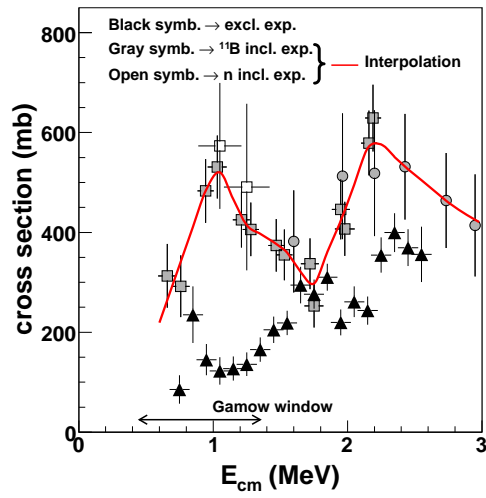


Fig. 1.— $^8\text{Li} + ^4\text{He} \rightarrow ^{11}\text{B} + n$ reaction cross section data versus E_{cm} : \square (La Cognata et al. 2008), \bullet (Boyd et al. 1992), \blacksquare (Gu et al. 1995), \blacktriangle (Ishiyama et al. 2006). The curve depicts the interpolated inclusive cross section σ_{incl} . The Gamow energy region at $T = 2 \times 10^9$ K is shown.

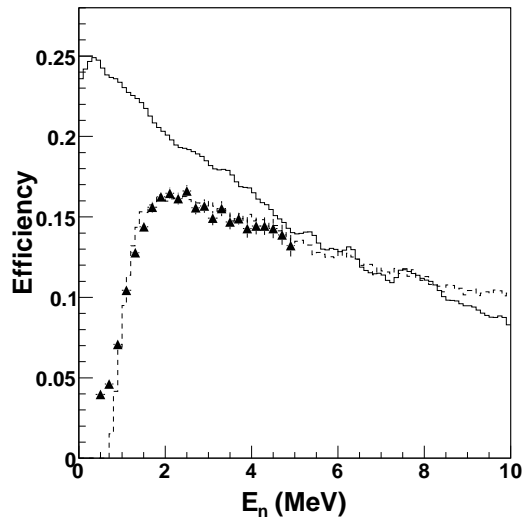


Fig. 2.— The dependence of the total detection efficiency of the thermalization counter in La Cognata et al. (2008) (solid histogram) and of the plastic scintillator arrays in Ishiyama et al. (2006); Hashimoto et al. (2006) (closed triangles) on the laboratory neutron energy. The dashed histogram is the Montecarlo simulation which better reproduces the efficiency data (Hashimoto et al. 2006).

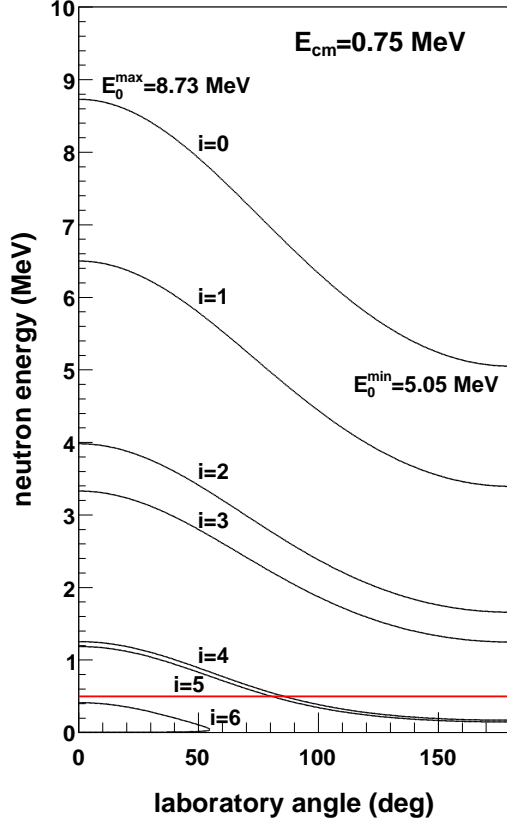


Fig. 3.— Kinematical plot showing the neutron energy-angle correlation for each branch of the ${}^8\text{Li} + {}^4\text{He} \rightarrow {}^{11}\text{B} + n$ reaction at $E_{cm} = 0.75$ MeV. The minimum and maximum neutron energies allowed by kinematics in the whole angular range are given for the $i = 0$ branch (${}^{11}\text{B}$ ground state). The red line represent the 0.5-MeV seeming cut on the neutron energy from Fig.2.

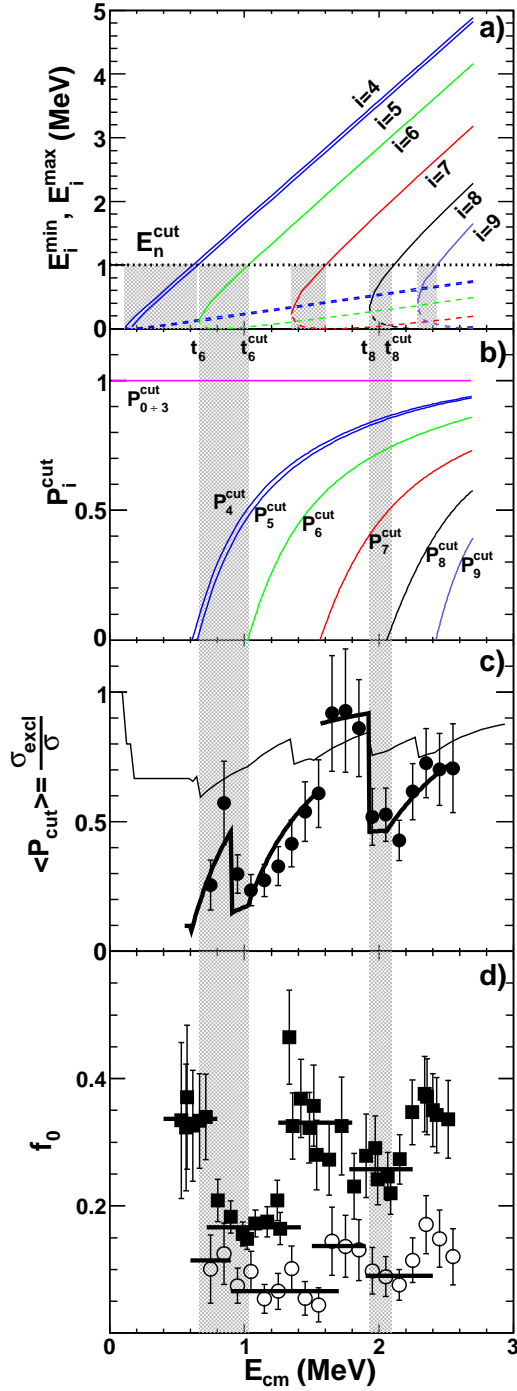


Fig. 4.— a) Kinematical loci of the minimum (dashed) and maximum (solid) laboratory neutron energies; b) the branch observability factors P_i^{cut} for $E_n^{cut} = 1$ MeV. The curves of the branches $i = 0 \div 3$, not shown above, are entirely above the $E_n^{cut} = 1$ MeV level and the corresponding $P_i^{cut} = 1$ independent of E_{cm} ; (c) the experimental $\langle P_{cut} \rangle$ (symbols), its best fit (thick curves) and the uniform pattern case (thin curve); (d) the branching ratio f_0 deduced from ground state cross section data in Ishiyama et al. (2006) (open circles) and Paradellis et al. (1990) (filled squares $\times 2$). The horizontal lines indicate the weighted mean f_0 values in the corresponding intervals.

Table 1: ^{11}B final state, center-of-mass reaction energy threshold t , observability energy threshold t^{cut} (assuming $E_n^{cut} = 1$ MeV), true branching ratios f in the indicated E_{cm} intervals and mean branching ratios $\langle f^{cut} \rangle$. Short lines indicate branching ratio values compatible with zero. Empty entries correspond to branches which are not physically open. In the fitting procedure, the $i = 0 \div 3$ branches are not separated and the summed $f_{0 \div 3}$ is given. The same applies to the $i = 4, 5$ branches.

i	State in ^{11}B $J^\pi, E^* \text{ (MeV)}$	t_i (MeV)	t_i^{cut} (MeV)	f_i				$\langle f_i^{cut} \rangle$	
				$0.75 \div 0.9 \text{ MeV}$	$0.9 \div 1.6 \text{ MeV}$	$1.6 \div 1.9 \text{ MeV}$	$1.9 \div 2.55 \text{ MeV}$	this work	Ref. (Ishiyama et al. 2006)
0	$\frac{3}{2}^-$	0.00	0						
1	$\frac{1}{2}^-$	2.12	0						
2	$\frac{5}{2}^-$	4.44	0						
3	$\frac{3}{2}^-$	5.02	0						
4	$\frac{7}{2}^-$	6.74	0.11						
5	$\frac{1}{2}^+$	6.79	0.16						
6	$\frac{5}{2}^+$	7.29	0.66						
7	$\frac{3}{2}^+$	7.98	1.35						
8	$\frac{3}{2}^-$	8.56	1.93						